



Stripes of increased diamagnetic susceptibility in underdoped superconducting $\text{Ba}(\text{Fe}_{1-x}\text{Co}_x)_2\text{As}_2$ single crystals: Evidence for an enhanced superfluid density at twin boundaries

B. Kalisky,^{1,2,*}† J. R. Kirtley,^{1,2,3} J. G. Analytis,^{1,2,4} Jiun-Haw Chu,^{1,2,4} A. Vailionis,^{1,4}
I. R. Fisher,^{1,2,4} and K. A. Moler^{1,2,4,5,*}‡

¹*Geballe Laboratory for Advanced Materials, Stanford University, Stanford, California 94305-4045, USA*

²*Department of Applied Physics, Stanford University, Stanford, California 94305-4045, USA*

³*IBM Watson Research Center, Route 134, Yorktown Heights, New York 10598, USA*

⁴*Stanford Institute for Materials and Energy Sciences, SLAC National Accelerator Laboratory, 2575 Sand Hill Road, Menlo Park, California 94025, USA*

⁵*Department of Physics, Stanford University, Stanford, California 94305-4045, USA*

(Received 11 August 2009; revised manuscript received 29 March 2010; published 17 May 2010)

Superconducting quantum interference device microscopy shows stripes of increased diamagnetic susceptibility in the superconducting state of twinned, orthorhombic, underdoped crystals of $\text{Ba}(\text{Fe}_{1-x}\text{Co}_x)_2\text{As}_2$, but not in tetragonal overdoped crystals. These stripes are consistent with enhanced superfluid density on twin boundaries.

DOI: [10.1103/PhysRevB.81.184513](https://doi.org/10.1103/PhysRevB.81.184513)

PACS number(s): 74.70.Xa, 74.62.Dh, 74.25.Ha, 74.62.Bf

The iron arsenide superconductors have critical temperatures T_c up to 57 K, multiband Fermi surfaces, and undoped parent compounds that have a paramagnetic to antiferromagnetic as well as a tetragonal to orthorhombic transition below temperatures of ~ 100 – 200 K. In $\text{Ba}(\text{Fe}_{1-x}\text{Co}_x)_2\text{As}_2$ and other members of the 122 family ($A\text{Fe}_2\text{As}_2$ with $A = \text{Ca}$, Sr , and Ba), doping causes the spin-density-wave transition temperature T_{SDW} and the structural transition temperature T_S to decrease,^{1,2} falling to zero at or near the doping where the highest T_c occurs, suggesting the importance of lattice changes in determining transport properties. Both experiment^{3–5} and theory⁶ have suggested a close relationship between structural and magnetic properties, leading some authors to describe the lattice and spin-density-wave transition by a single order parameter.^{7,8} In addition, structural strain appears to play a significant role in the superconductivity. For example, in the 122 compounds, small amounts of nonhydrostatic pressure can induce superconductivity.^{9–13} In addition, there is evidence that the structural perfection of the Fe-As tetrahedron is important for the high critical temperatures observed in the Fe pnictides.^{14,15} In the present work, we find evidence for the importance of a particular structural formation, a twin boundary, in *increasing* the superfluid density. Imaging the local diamagnetic susceptibility (Fig. 1) of single crystals of underdoped (UD) $\text{Ba}(\text{Fe}_{1-x}\text{Co}_x)_2\text{As}_2$ ($x < 0.07$), we find a striped pattern for $T \leq T_c$, consistent with a large enhancement of the superfluid density on the twin boundaries.

The crystal growth is described in Ref. 1. Superconductivity is induced by substituting Co onto the Fe site¹⁶ with optimal doping occurring at $x \sim 0.07$. We use a variable- T scanning superconducting quantum interference device (SQUID) susceptometer^{17–19} with two field coil/pickup loop pairs in a gradiometer configuration. One field coil/pickup loop pair is scanned over the sample [Fig. 1(a) overlay sketch]. In the more common measurement mode of scanning SQUID magnetometry, there is no field from the field coil, and the images of the flux through the pickup loop indicate the local magnetic field of the sample integrated

over the pickup loop area. In the scanning SQUID *susceptometry* images shown in this paper, an ac current in the field coil creates a local applied field. The resulting total ac flux through the SQUID pickup loop includes the contribution from the magnetic field generated by the sample in response.

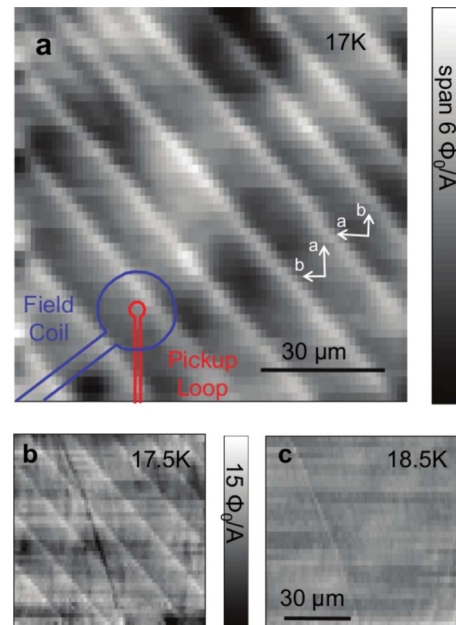


FIG. 1. (Color online) Local susceptibility image in underdoped $\text{Ba}(\text{Fe}_{1-x}\text{Co}_x)_2\text{As}_2$, indicating increased diamagnetic shielding on twin boundaries. (a) Local diamagnetic susceptibility, at $T=17$ K, of the ab face of sample UD1 ($x=0.051$ and $T_c=18.25$ K), showing stripes of enhanced diamagnetic response (white). In addition there is a mottled background associated with local T_c variations that becomes more pronounced as $T \rightarrow T_c$. Overlay: sketch of the scanning SQUID's sensor. The size of the pickup loop sets the spatial resolution of the susceptibility images. [(b) and (c)] Images of the same region at (b) $T=17.5$ K and (c) at $T=18.5$ K show that the stripes disappear above T_c . A topographic feature (scratch) appears in (b) and (c).

TABLE I. Details of samples that were measured by scanning SQUID microscopy. UD, OD, and OPD stand for underdoped, overdoped, and optimally doped. T_c (superconducting transition) was measured *in situ* and T_{SDW} and T_S (magnetic and structural transitions) were determined by the temperature derivatives of resistivity. Stripes of stronger magnetic susceptibility were observed only in underdoped samples.

Name	Doping (%)	T_c (K)	T_{SDW} (K)	T_S (K)	Observed
UD1	5.1	18.25 ± 0.25	36.8 ± 7	55 ± 5	Stripes
UD2	4.5	12.75 ± 0.5	57.3 ± 4	69.5 ± 2	Stripes
UD3	5.1	18.25 ± 0.25	36.8 ± 7	55 ± 5	Stripes
UD4	4.5	12.25 ± 1	57.3 ± 4	69.5 ± 2	Stripes
OD1	8.5	19.9 ± 0.1			
OD2	8.5	20.2 ± 0.1			
OPD1	6.1	22.8 ± 0.1			

The mutual inductance of each pair is defined as the ratio of the ac flux through the pickup loop divided by the ac current through the field coil. Each pair has a mutual inductance $800\Phi_0/A$, where $\Phi_0 = h/2e$ is the superconducting flux quantum, in the absence of a sample. When one field coil/pickup loop pair is scanned close to a sample, the inductance of that pair is modified by an amount χ , due to the sample's local magnetic susceptibility. The data shown here were taken with a 0.25 mA ac current in the field coil, which would generate a field of ~ 1.5 Gauss at the surface of the sample in the absence of screening. We have checked that all data in this paper are within the linear-response regime.

The exact relationship of χ to the local magnetic penetration depth λ and superfluid density $n_s \sim 1/\lambda^2$ is determined by the sample and sensor geometry as described in Refs. 17–20. For a uniform sample in the limit of small n_s , $\chi \propto n_s^{3/2}$. The spatial resolution is primarily determined by the pickup loop diameter (4 μm), although the field coil diameter (17 μm) and sample-sensor separation (1–2 μm) also play a role.

We observe lines of enhanced diamagnetic susceptibility, henceforth called “stripes,” along the orthorhombic $[110]$ or $[1\bar{1}0]$ crystalline directions. The orientation of the samples was determined *in situ* by imaging crystal edges, which naturally cleaved along the $[100]$ or $[010]$ directions. A susceptibility image of a region of sample UD1 is shown in Fig. 1(a). These stripes are observed only below the superconducting transition as shown by Figs. 1(b) and 1(c), taken below and above T_c . The spacing of the stripes varies between 10–16 μm in Fig. 1, up to 35 μm in other parts of this sample (UD1), and down to < 1 μm in parts of other samples (UD2–4).

The orientation of the observed stripes is consistent with the expected direction of the twin boundaries occurring in underdoped $\text{Ba}(\text{Fe}_{1-x}\text{Co}_x)_2\text{As}_2$ below the tetragonal to orthorhombic structural transition at $T_S \sim 55$ to 70 K (Table I). The crystal structure and one possible twin boundary configuration are sketched in Figs. 2(a)–2(d). Local optical polarization measurements (POL) on the undoped parent compound BaFe_2As_2 (Ref. 21 and Table II) and on doped samples (Refs. 22 and 23) have confirmed that the twin boundaries

form in parallel lines with a range of spacings. We suspect that the spacing of twin boundaries depends on sample geometry and on the method of sample mounting in addition to the doping dependence of the orthorhombicity.²⁴

We suggest that we are imaging twin boundaries and check this hypothesis in three ways. First, we checked the behavior of the stripes on thermal cycling (Fig. 3). On increasing the temperature T above T_c , the stripes disappear,

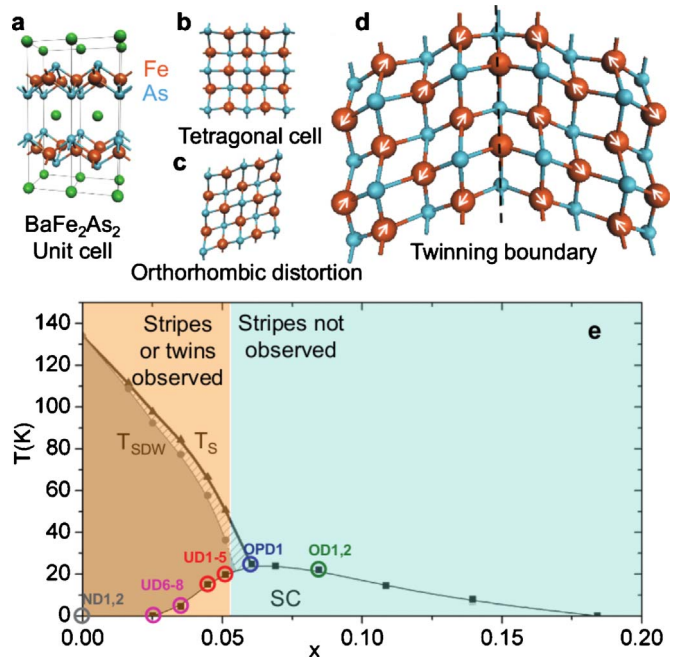


FIG. 2. (Color online) Sketches of (a) BaFe_2As_2 unit cells in the (b) tetragonal and (c) orthorhombic phases (orthorhombic distortion exaggerated for clarity and three-dimensional projection view used to convey the out-of-plane locations of the arsenides). (d) Possible twin boundary configuration. Spins on the Fe sites are drawn in the configuration that they would have in the absence of the twin boundary. (e) The phase diagram of the electron-doped superconductor $\text{Ba}(\text{Fe}_{1-x}\text{Co}_x)_2\text{As}_2$ modified from Ref. 1. The samples measured in this work are marked by circles and the orange shaded area below $x=0.051$ marks the region where stripes or twin boundaries were observed in these samples.

TABLE II. Details of samples that were shown to form twins by structural techniques. XRD stands for x-ray diffraction and POL for optical polarization measurements. UD and ND stand for underdoped and nondoped. T_c (superconducting transition) was measured by susceptibility using Quantum Design 5T magnetic properties measurement system (MPMS). T_{SDW} and T_S (magnetic and structural transitions) were determined by the temperature derivatives of resistivity. All samples were shown to form twins.

Name	Doping (%)	T_c (K)	T_{SDW} (K)	T_S (K)	Tool
ND1	0		134 ± 0.5	134 ± 0.5	XRD
UD5	5.1	18.7 ± 0.25	36.8 ± 7	55 ± 5	XRD
UD6	2.5		92.2 ± 0.7	98.5 ± 1	XRD
ND2	0		134 ± 0.5	134 ± 0.5	POL
UD7	2.5		92.2 ± 0.7	98.5 ± 1	POL
UD8	3.5	4.6 ± 3.2	77.3 ± 2	86.7 ± 2	POL

but reappear in the same locations once T is decreased [Figs. 3(a)–3(c)]. However, when warmed above T_S and recooled, some of the stripes reappear in different locations [Figs. 3(d)–3(f)]. The scratchlike defect, probably topographic, that can be seen in Figs. 1(b), 1(c), and 3(b) serves as a marker to verify that the scan area does not drift. Such location variation on thermal cycling to this temperature is naturally expected for twin boundaries formed at the orthorhombic transition but not expected for other structural defects (such as dislocations).

Second, we determined the doping dependence [see Fig. 2(e)]. Four UD samples, two with $x=5.1\%$ and two with $x=4.5\%$ all showed stripes. We also studied one optimally doped (OPD) sample ($x=6.1\%$) and two overdoped (OD) samples ($x=8.5\%$), neither of which had stripes. The properties of the samples studied using scanning SQUID magnetometry and susceptometry are summarized in Table I. The observed doping dependence is consistent with stripes being associated with twin boundaries since it does not show stripes in samples that do not undergo the tetragonal transition.

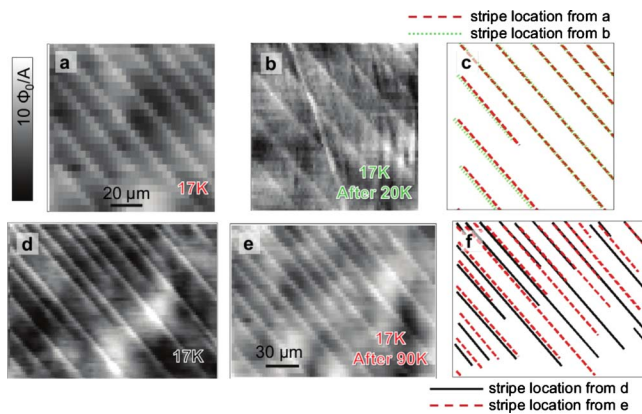


FIG. 3. (Color online) Effect of thermal cycling on the locations of the stripes. [(a)–(c)] Local susceptibility images at 17 K (a) before and (b) after thermal cycling to $T=20$ K, above T_c but below $T_{S/SDW}$, show (c) unchanged stripe locations for all stripes. [(d)–(f)] Images (d) before and (e) after thermal cycling to 90 K, above $T_{S/SDW}$, show (f) changed stripe locations for most stripes. This figure shows overlapping regions representative of much larger regions imaged under similar conditions.

Finally, we made T -dependent powder x-ray diffraction (XRD) measurements on samples from $x=0\%$ to 5.1% , which confirmed the existence of the tetragonal to orthorhombic phase transition at a doping-dependent T from 135 to 55 K. We also confirmed the existence of a structural phase transition on three single-crystal samples with dopings of 0%, 2.5%, and 5.1% using spatially resolved single-crystal x-ray diffraction with a square beam $5\text{--}10 \mu\text{m}$ across. We confirmed that each sample in Table II (ND1–2, UD5–8) forms twins.

Figure 4 shows the temperature dependence of the total susceptibility and amplitude of the stripes of sample UD3. As expected, χ decreases with increasing T until it disappears at T_c , where λ diverges. The locally measured T_c

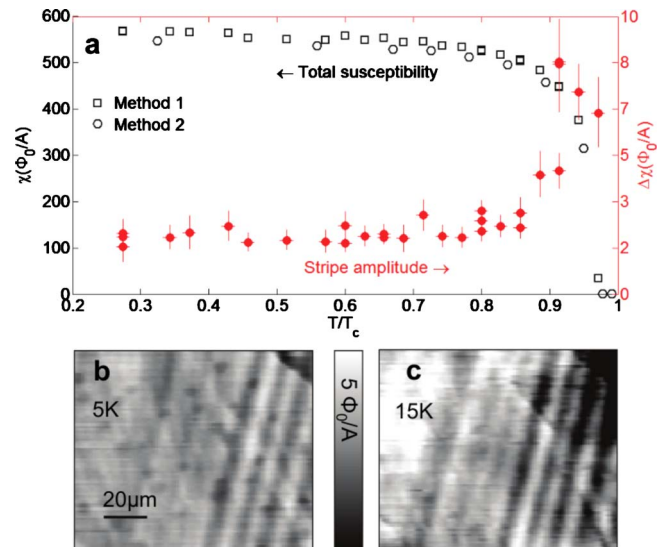


FIG. 4. (Color online) (a) Temperature dependence of the local diamagnetism. (Left axis) Typical susceptibility signal $\chi(T)$ in sample UD3 vs T/T_c , measured as the difference between the susceptibility high above the sample and in contact at a specific location (method 1) or averaged over a region of the sample (method 2). (Right axis) Amplitude for stripes $\Delta\chi(T)$ in UD3 [stripes shown in (b) and (c)]. T is scaled by the local $T_c=18$ K. [(b) and (c)] Susceptometry images of UD3 at (b) 5 K and (c) 15 K. Dark disks at the vortex locations (b) are artifacts related to nonlinearity in the SQUID feedback loop at this set point.

typically varied by $\sim \pm 0.25$ K for different regions of the samples with $x=5.1\%$ (UD1, UD3, and UD5), by $\sim \pm 1$ K for samples with $x=4.5\%$ (UD2 and UD4), and by $\sim \pm 0.1$ K for samples with $x=6.1\%$ and 8.5% (OD1, OD2, and OPD1). An increase in the variation in T_c within samples is expected in underdoped samples because of the stronger dependence of the average T_c on doping for these samples [Fig. 2(e)].

The magnitude of the susceptibility signal associated with the stripes $\Delta\chi(T)$ is shown in Fig. 4(a). $\Delta\chi(T)$ was obtained by fitting χ from the sample area on the right side of Figs. 4(b) and 4(c) to the model described in Ref. 25 as a function of temperature. $\Delta\chi_{\text{stripe}} \sim 2-6\Phi_0/A$ is comparable to the bulk susceptibility signal close to T_c but much smaller than the saturated bulk susceptibility $\chi_{\text{sample}} \sim 600\Phi_0/A$ at lower T . We believe that the enhanced susceptibility stripes are associated with enhanced superfluid density on the twin planes. As can be seen from Fig. 1, and from the cross sections displayed in Ref. 25, the stripes in susceptibility are sharply peaked at the positions corresponding to enhanced superfluid density, and more rounded at positions corresponding to lower superfluid density. It is difficult to understand how such sharp, resolution-limited features in susceptibility could arise if they are not on the twin boundaries, given that, as we have shown, they are associated with the formation of twin boundaries. Reference 25 calculates the change in susceptibility due to an embedded sheet of reduced penetration depth for a geometry that is relevant to this case (the sheet is on the a - b twin plane, extended through the crystal along the c axis). The values for the enhancement of the Cooper pair density on the sheets, estimated by this model, are between 10^{19} and 10^{20} m^{-2} . As discussed in the accompanying modeling paper,²⁵ it is difficult to determine the enhancement of the volume density of Cooper pairs along the twin boundary planes because of our uncertainty in the widths of the regions of enhanced superfluid density. For comparison, the two-dimensional electron liquid at the $\text{SrTiO}_3/\text{LaAlO}_3$ interface, which becomes superconducting with a critical temperature of 0.2 K, has a carrier concentration of about 10^{17} m^{-2} .²⁶ We did not observe stripes above T_c , possibly because of fluctuations.

The above measurements are consistent with a substantial enhancement of superfluid density on the twin boundaries in underdoped $\text{Ba}(\text{Fe}_{1-x}\text{Co}_x)_2\text{As}_2$. Variation in chemical doping across the twin boundaries is unlikely because the structural transition occurs below 100 K where the diffusion of chemical dopants is expected to be extremely low, although detailed annealing studies would be needed to determine the mobility of the impurities. Phonon softening at twin boundaries has been proposed to explain enhancement of conventional pairing and as an explanation for a T_c increase in elemental Nb and Sn.²⁷ However, conventional electron-phonon coupling alone cannot explain the T_c of the pnictides.²⁸ Recently, there were proposals for more exotic pairing scenarios that involve the local structure and mag-

netic environment.^{6,29} In Fig. 2(d) we have drawn the colinear antiferromagnetic ordering of the Fe spins below T_{SDW} (50–70 K) in the configuration they would have without the twin boundary. It is clear that along the twin boundaries the spin orientation is ill defined, which may enhance spin-fluctuation-mediated pairing along the boundary.

We also noticed that vortices tended not to pin on top of the stripes in our experimental conditions and could not be dragged across stripes using SQUID sensors or magnetic force microscopy tips. We believe that both the enhancement in superfluid density and the barrier to vortex motion by the stripes may be mechanisms for enhanced critical currents in twinned samples.

In conclusion, we have measured the local diamagnetic susceptibility of underdoped samples of $\text{Ba}(\text{Fe}_{1-x}\text{Co}_x)_2\text{As}_2$ and have observed an enhancement of the superfluid density along stripes. These stripes occur in the direction and with the regularity known for twinning boundaries forming below the structural transition of the parent compounds. The thermal and doping behavior of the stripes is consistent with that of twinning boundaries and so we conclude that the superfluid enhancement occurs along these structural defects. We therefore provide a direct observation for the important role of crystalline and/or magnetic structures in the superconductivity of the Fe pnictides. These widely separated, naturally occurring sheets of enhanced superfluid density give a unique opportunity to access superconductivity in its two-dimensional limit. These results demonstrate the ability of spatially resolved susceptibility measurements to determine the relationship between local structure and an important parameter characterizing the superconductivity, namely, the superfluid density.

ACKNOWLEDGMENTS

We would like to thank O. M. Auslaender, Lan Luan, A. Auerbach, and A. Vishwanath for useful discussions. This work was supported by the Department of Energy (DOE) under Contract No. DE-AC02-76SF00515, by NSF under Grant No. PHY-0425897, and by the U.S.-Israel Binational Science Foundation. B.K. acknowledges support from L’Oreal USA for Women in Science. J.R.K. was partially supported with a Humboldt Forschungspreis. Single crystal x-ray diffraction was performed at HPCAT (Sector 16), Advanced Photon Source (APS), Argonne National Laboratory. HPCAT was supported by DOE-BES, DOE-NNSA, NSF, and the W.M. Keck Foundation. APS is supported by DOE-BES, under Contract No. DE-AC02-06CH11357. Powder x-ray diffraction was carried out at Stanford Synchrotron Radiation Laboratory, a national user facility operated by Stanford University on behalf of the U.S. Department of Energy, Office of Basic Energy Sciences. We thank Wenge Yang for the support of the single crystal x-ray diffraction measurements, and A. S. Erickson, C. L. Condon, and M. F. Toney for their support of the powder x-ray diffraction experiments.

*Authors to whom correspondence should be addressed.

[†]beena@stanford.edu

[‡]kmoler@stanford.edu

- ¹J. H. Chu, J. G. Analytis, C. Kucharczyk, and I. R. Fisher, *Phys. Rev. B* **79**, 014506 (2009).
- ²N. Ni, M. E. Tillman, J. Q. Yan, A. Kracher, S. T. Hannahs, S. L. Bud'ko, and P. C. Canfield, *Phys. Rev. B* **78**, 214515 (2008).
- ³S. A. J. Kimber, A. Kreyssig, Y. Z. Zhang, H. O. Jeschke, R. Valenti, F. Yokaichiya, E. Colombier, J. Yan, T. C. Hansen, T. Chatterji, R. J. McQueeney, P. C. Canfield, A. I. Goldman, and D. N. Argyriou, *Nature Mater.* **8**, 471 (2009).
- ⁴R. H. Liu, T. Wu, G. Wu, H. Chen, X. F. Wang, Y. L. Xie, J. J. Ying, Y. J. Yan, Q. J. Li, B. C. Shi, W. S. Chu, Z. Y. Wu, and X. H. Chen, *Nature (London)* **459**, 64 (2009).
- ⁵W. E. Pickett, *Nat. Phys.* **5**, 87 (2009).
- ⁶T. Yildirim, *Phys. Rev. Lett.* **102**, 037003 (2009).
- ⁷C. Fang, H. Yao, W. F. Tsai, J. P. Hu, and S. A. Kivelson, *Phys. Rev. B* **77**, 224509 (2008).
- ⁸C. Xu, M. Muller, and S. Sachdev, *Phys. Rev. B* **78**, 020501 (R) (2008).
- ⁹E. Colombier, S. L. Bud'ko, N. Ni, and P. C. Canfield, *Phys. Rev. B* **79**, 224518 (2009).
- ¹⁰A. I. Goldman, A. Kreyssig, K. Prokes, D. K. Pratt, D. N. Argyriou, J. W. Lynn, S. Nandi, S. A. J. Kimber, Y. Chen, Y. B. Lee, G. Samolyuk, J. B. Leao, S. J. Poulton, S. L. Bud'ko, N. Ni, P. C. Canfield, B. N. Harmon, and R. J. McQueeney, *Phys. Rev. B* **79**, 024513 (2009).
- ¹¹A. Kreyssig, M. A. Green, Y. Lee, G. D. Samolyuk, P. Zajdel, J. W. Lynn, S. L. Bud'ko, M. S. Torikachvili, N. Ni, S. Nandi, J. B. Leao, S. J. Poulton, D. N. Argyriou, B. N. Harmon, R. J. McQueeney, P. C. Canfield, and A. I. Goldman, *Phys. Rev. B* **78**, 184517 (2008).
- ¹²W. Yu, A. A. Aczel, T. J. Williams, S. L. Bud'ko, N. Ni, P. C. Canfield, and G. M. Luke, *Phys. Rev. B* **79**, 020511(R) (2009).
- ¹³P. L. Alireza, Y. T. C. Ko, J. Gillett, C. M. Petrone, J. M. Cole, G. G. Lonzarich, and S. E. Sebastian, *J. Phys.: Condens. Matter* **21**, 012208 (2009).
- ¹⁴J. Zhao, Q. Huang, C. de la Cruz, S. Li, J. W. Lynn, Y. Chen, M. A. Green, G. F. Chen, G. Li, Z. Li, J. L. Luo, N. L. Wang, and P. Dai, *Nature Mater.* **7**, 953 (2008).
- ¹⁵C.-H. Lee, A. Iyo, H. Eisaki, H. Kito, M. T. Fernandez-Diaz, T. Ito, K. Kihou, H. Matsuhata, M. Braden, and K. Yamada, *J. Phys. Soc. Jpn.* **77**, 083704 (2008).
- ¹⁶A. S. Sefat, R. Y. Jin, M. A. McGuire, B. C. Sales, D. J. Singh, and D. Mandrus, *Phys. Rev. Lett.* **101**, 117004 (2008).
- ¹⁷B. W. Gardner, J. C. Wynn, P. G. Bjornsson, E. W. J. Straver, K. A. Moler, J. R. Kirtley, and M. B. Ketchen, *Rev. Sci. Instrum.* **72**, 2361 (2001).
- ¹⁸M. E. Huber, N. C. Koshnick, H. Bluhm, L. J. Archuleta, T. Azua, P. G. Bjornsson, B. W. Gardner, S. T. Halloran, E. A. Lucero, and K. A. Moler, *Rev. Sci. Instrum.* **79**, 053704 (2008).
- ¹⁹J. R. Kirtley, C. C. Tsuei, K. A. Moler, V. G. Kogan, J. R. Clem, and A. J. Turberfield, *Appl. Phys. Lett.* **74**, 4011 (1999).
- ²⁰V. G. Kogan, *Phys. Rev. B* **68**, 104511 (2003).
- ²¹M. A. Tanatar, A. Kreyssig, S. Nandi, N. Ni, S. L. Bud'ko, P. C. Canfield, A. I. Goldman, and R. Prozorov, *Phys. Rev. B* **79**, 180508(R) (2009).
- ²²R. Prozorov, M. A. Tanatar, N. Ni, A. Kreyssig, S. Nandi, S. L. Bud'ko, A. I. Goldman, and P. C. Canfield, *Phys. Rev. B* **80**, 174517 (2009).
- ²³J. Chu, J. Analytis, D. Press, K. De Greve, T. Ladd, Y. Yamamoto, and I. Fisher, [arXiv:0911.3878](https://arxiv.org/abs/0911.3878) (unpublished).
- ²⁴S. Nandi, M. G. Kim, A. Kreyssig, R. M. Fernandes, D. K. Pratt, A. Thaler, N. Ni, S. L. Bud'ko, P. C. Canfield, J. Schmalian, R. J. McQueeney, and A. I. Goldman, *Phys. Rev. Lett.* **104**, 057006 (2010).
- ²⁵J. Kirtley, B. Kalisky, L. Luan, and K. Moler, following paper, *Phys. Rev. B* **81**, 184514 (2010).
- ²⁶N. Reyren, S. Thiel, A. D. Caviglia, L. F. Kourkoutis, G. Hammerl, C. Richter, C. W. Schneider, T. Kopp, A. S. Ruetschi, D. Jaccard, M. Gabay, D. A. Muller, J. M. Triscone, and J. Mannhart, *Science* **317**, 1196 (2007).
- ²⁷I. N. Khlyustikov and A. I. Buzdin, *Adv. Phys.* **36**, 271 (1987).
- ²⁸L. Boeri, O. V. Dolgov, and A. A. Golubov, *Phys. Rev. Lett.* **101**, 026403 (2008).
- ²⁹I. I. Mazin and M. D. Johannes, *Nat. Phys.* **5**, 141 (2009).